Intelligent Medical Diagnostic System for Osteoarthritis: A Deep Learning Approach and Comparison

Prof. Ayesha Asif Sayyad[1], Dr. Rajesh Keshavrao Deshmukh[2]
[1]*Pune University, Pune, Maharashtra, India,*
[2]*Kalinga University, Naya Raipur, Chhattisgarh, India*

Osteoarthritis (OA) is a disabling joint disease, predominantly affecting the elderly and the obese, and resulting in compromised quality of life and heightened frailty. This review article addresses the existing diagnostic techniques employed in OA that largely depend upon clinical examination and imaging techniques. These techniques might be deficient in efficiency and accuracy, therefore, such complicated diagnostic systems are required. This article suggests an Intelligent Medical Diagnostic System for Osteoarthritis based on deep learning and medical imaging. Combing medical images and deep features, the system will identify and classify OA, especially of the knee joint, appropriately. The problems regarding irrelevant feature selection and database management issues of large databases are solved, as well as research on Magnetic Resonance Imaging (MRI) methods for detection and OA classification. The review offers detailed discussion on location strategy, feature extraction methods, and classification models suitable for OA diagnosis, and provides recent development and future direction.

***Index Terms*- OA, Classification Methods, Deep Learning, Feature extraction, Medical Imaging, MRI.**

I. INTRODUCTION

Arthritis is a prevalent public health condition with different forms including Osteoarthritis (OA), Rheumatoid Arthritis (RA), Gout, and Juvenile Arthritis (JA). All the forms of arthritis pose diagnostic and management challenges, the most prevalent being OA, which tends to develop due to cartilage degeneration in the joint and the bone underneath [1]. Medical imaging, spearheaded by MRI, plays a crucial role in the diagnosis and follow-up of arthritis. Problems such as noise, artifacts, and lack of proper contrast in MR images can be pesky, and hence hamper proper analysis. Intelligent Medical Diagnostic Systems (IMDS) have surfaced as effective tools to improve the quality of MR images that are used for the diagnosis of arthritis [2]. Techniques such as SANR_CNN and MultiResUNet architectures are being explored to further enhance image denoising, segmentation, and feature extraction [3]. The technologies aim at overcoming the challenges in knee MR image analysis, minimizing the need for manual intervention, and maximizing the accuracy of arthritis diagnosis [4]. Application of AI in radiology can further be utilized for automating the classification process, especially for knee OA and other diseases, which results in better patient outcomes and effective healthcare provision. In an effort to circumvent the weaknesses of manual and semi-automatic analysis of knee MR images, automated systems are now being created in greater numbers in order to achieve better accuracy and less variability in diagnosis [5]. For example, bone segmentation of knee MR images with the MultiResUNet model comprises a multi-stage design with preprocessing for correcting noise and contrast, extraction of bone area, and boundary smoothing [6]. These intelligent medical diagnostic system and AI technologies are ready to advance early diagnosis and management of diseases such as OA, lower healthcare expenditures, and better patient outcomes through more reliable and precise diagnostic processes [7].

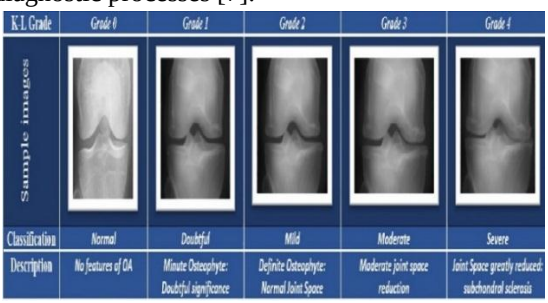

Figure 1: KL grading stages for knee OA [8]

Osteoarthritis (OA) is among the most common chronic rheumatic conditions worldwide, exacting huge pain and disability burdens across many

countries. Described by the Osteoarthritis Research Society International (OARSI) as a condition that affects mobile joints, OA begins with cell stress and extracellular matrix breakdown, usually initiated by micro- and macro-trauma [9]. Such degradation initiates maladaptive repair responses, most significantly pro-inflammatory processes of innate immunity, culminating in a cascade of molecular [10], anatomical, and physiological derangements of affected joints. The three most significant symptoms of OA are pain, stiffness, and limited movement of involved joints [11]. Pain develops during activity and initially, only upon it; as OA disease evolves, though, discomfort will become evident even in the setting of rest. The impairment of the normal joint function, defined by cartilage breakdown, bone remodeling, osteophyte growth, and inflammation of the joint, highlights the gradual nature of OA, ultimately leading to joint deformity and inflammation [12]. Although OA pervasively affects joints like the knee, hip, foot, spine, and hand, its influence transcends these areas, potentially affecting any movable joint in the body. In spite of lack of direct action on other tissues and organs within the body, patients with OA frequently struggle with comorbidities that demand comprehensive management schemes [13].

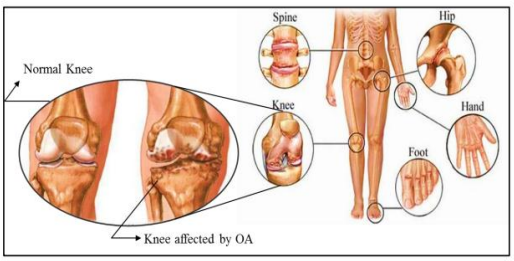

Figure 2: Knee affected by OA [13]

Concurrently, rheumatoid arthritis (RA) is another prominent form of arthritis, with autoimmune derangement and chronic inflammation but synovial joint predilection. In contrast to OA [14], RA results in joint structure destruction and is typically accompanied by systemic symptoms, including pain, swelling, and stiffness in several joints. The pathophysiology of RA transcends the boundaries of genetic susceptibility, and factors like thickness of cartilage, volume of synovial fluid, and tissue content enter into the arena of the multi-factorial interaction of disease and symptomatology [15]. Similar to OA, the prognosis and treatment of RA also demonstrate extreme heterogeneity in sufferers, ranging from no symptoms to incapacitating disability [16]. The present thesis purports to discuss the use of deep learning models to diagnose OA, providing insights on the design, development, and testing of a smart diagnosis system specifically in respect of this highly complex disease's distinctive challenge [17]. By interdisciplinary collaboration and creative technological innovations, this study seeks to contribute to the progress of medical science and the provision of personalized healthcare interventions for people suffering from OA [18].

A. Noise Distribution

In general, Gaussian noise degrades medical MR pictures, which are simple to deal with and are signal dependent. The visual quality and quantitative features are impeded by the noise. The Gaussian noise disrupts the gray value in medical MR images, the distribution function is shown in equation [19].

$$P(G) = \frac{1}{\sigma\sqrt{2\pi}} - e^{\frac{(i-\mu)^2}{2\sigma^2}}$$

where, i is gray intensity, σ is standard deviation, μ is average value. The Rician noise is represented as in equation 3.2.

$$R(n) = Y_i + Y_o$$

Where, Yi, and Yo, are imaginary and original values.

$$Y_i = ICos\theta + \omega_1$$

$$Y_o = ISin\theta + \omega_2$$

B. Epidemiology of Knee

This section presents a summary of the epidemiological evidence on the incidence of osteoarthritis (OA), more specifically knee OA, in light of different factors that contribute to it [20]. OA is a joint degenerative condition that usually affects older adults and is more frequent in women than in men [21]. Although it may occur in any joint of the body, such as the spine, fingers, hips, and toes, knee OA is among the most prevalent. All over the world, OA impacts a large percentage of the population and is estimated at 240 million affected individuals. With the ageing of the population [22], OA will increase, notably in women and people aged 60 years or more. The percentage of the population above the age of 65 years will double in two decades in most Asian nations where the population is ageing very quickly. This population change is expected to add to the increased

prevalence of OA in the region [23]. Of particular note, in India, OA prevalence has been cited at between 22% and 39%, with knee OA reaching an estimated 28.7% prevalence among the population. Prevalence of OA varies with factors including gender, weight, lifestyle, and habitat. For example, knee OA has a greater occurrence in women than in men and is greater in urban areas as well as higher BMI individuals [10]. Sedentary lifestyle is another reason contributing to higher knee OA prevalence. The epidemiologic statistics show the growing knee OA incidence worldwide and deserve to become well-acquainted with its anatomy and symptoms associated. Knee OA is related to progressive cartilage loss in the joint, which remains a most important parameter in joint function [24]. Therefore, an accurate knowledge of knee OA anatomy and the definition of knee OA is most important for its early diagnosis and treatment. Epidemiological evidence in this section also indicates the enormous public health burden of knee OA worldwide and the need for more research and interventions to curtail this emerging public health issue. By understanding the etiology of knee OA and its impact on the quality of life of the individuals involved, healthcare workers can formulate successful prevention, diagnosis, and treatment programs for this disabling condition [25].

C. Knee Anatomy

Knee joint is a combination of several tissues consisting of bones, cartilages, meniscus, ligaments, tendons, and joint capsule [26]. Accurate knowledge about the anatomy of knee joint is required in the understanding of the pathophysiology of osteoarthritis (OA), a common degenerative arthritis that occurs in millions of people worldwide [27]. The knee joint is basically constituted by the three bones of articulation, which are the femur (thigh bone), the tibia (shinbone), and the patella (kneecap). The bones are supported and held in place by a highly complicated system of muscles, tendons, and ligaments [28]. The joint in the knee is stabilized by a fibrous joint capsule that holds and supports synovial fluid for lubrication and delivery of nutrients to the articular surfaces. Of these tissues engaged in knee function and impact by OA, most vital are bone and cartilage [29]. Cartilage, in the form of articular cartilage, covers the ends of bones within the joint and a smooth low-friction surface for frictionless gliding. Cartilage consists primarily of chondrocyte cells suspended in an elastin and collagen fiber matrix gel. Cartilage is tough, but also malleable, and ideal for weight-bearing uses [30]. It has no blood supply or nerve endings, though, like bone, and is hence less self-repairing. As such, cartilage injury or degradation can lead to pain, stiffness, and restricted joint function. Bone, on the other hand, is a living tissue with an extensive blood supply and remarkable capacity to repair itself. Bone gives the body structural support and is also the point of attachment of muscles [31], tendons, and ligaments. Subchondral sclerosis (bone hardening beneath cartilage), bone spurs or osteophytes, and cysts are seen in knee OA. These are generally found in high grades of OA and contribute to disability in function and pain. Progressive degeneration of cartilage is the universal finding in knee OA [32]. When there is erosion of cartilage, underlying bone becomes exposed and remodels under altered mechanical stresses. The remodeling causes osteophyte formation, joint deformity, and even loss of function of the joints. Awareness regarding the intricate interconnection between cartilage and bone of the knee joint is critical while developing treatment strategies for OA. Though current therapy is symptom-managed and there is an attempt to preserve the functional joint, research also continues to seek alternative therapeutic targets through which to reverse or arrest this degenerative process. The knee joint is a complex composite of bone, cartilage, and other stabilizing tissues [33]. In OA, progressive cartilage loss and bone change result in pain, stiffness, and decreased mobility. By further understanding knee anatomy and OA pathophysiology, clinicians and researchers can advance more specifically towards more personalized and targeted treatments for this elusive disease.

II. RELATED WORK

Table 1: Literature Survey

Author(s)	Title / Focus, Methodology, Key Findings
Neha Sharma et.al (2024) [7]	Comprehensive review of arthritis, focusing on KOA and machine learning-based detection methods Methodology Review of KOA and ML-based diagnostic methods Key Findings Early KOA detection improved with ML-based approaches

Suman Rani et.al (2024) [34]	Deep learning-based KOA detection using a 12-layer CNN with high classification accuracy Methodology 12-layer CNN, OAI dataset, KL grading Key Findings 92.3% accuracy in binary classification, 78.4% in multi-class classification
P. M. Dinesh et.al (2024) [35]	Systematic framework using CNNs and RNNs for knee osteoarthritis prediction Methodology CNNs, RNNs, image recognition and segmentation Key Findings Significant improvement in KOA diagnosis using CNN and RNN
YUN XIN TEOH et.al (2024) [13]	Survey of XAI techniques for explainability in AI-based knee OA diagnosis Methodology XAI techniques, GradCAM, SHAP Key Findings 89.7% of AI studies employed XAI techniques for transparency
RAFIQUE AHMED et.al (2024) [36]	Exploration of deep learning models and interpretability for KOA classification Methodology SOTA deep learning models, interpretability via GradCAM Key Findings Binary-class classification improves model interpretability
Ji Soo Yoon et.al (2023) [37]	Development and validation of an AI model for JSN quantification and osteophyte detection Methodology AI model for JSN quantification, KL grade classification Key Findings Validated AI model for JSN quantification and osteophyte detection

AMJAD REHMAN et.al (2024) [38]	Deep learning-based CNN model for early KOA diagnosis using X-ray images Methodology Deep learning CNN, X-ray image-based KOA diagnosis Key Findings Improved KOA diagnosis through CNN-based deep learning
Muhammad Attique Khan et.al (2023) [39]	Human gait analysis for KOA prediction using deep learning techniques Methodology Gait analysis using deep learning for KOA assessment Key Findings Deep learning improves KOA prediction from human gait analysis
Jiangling Song et.al (2023) [40]	KOA diagnosis using vibroarthrographic signals and deep learning models Methodology VAG signals, deep learning for KOA diagnosis Key Findings New KOA-CAD system using multivariate deep learning
Yun Xin Teoh et.al (2022) [5]	Review of imaging modalities and machine learning approaches for knee OA Methodology Machine learning on imaging features from X-rays and MRIs Key Findings MRI-based imaging features are critical for KOA diagnosis
S. Sheik Abdullah et.al (2024) [41]	KOA detection using Faster RCNN and ResNet-50 for feature extraction Methodology Faster RCNN, ResNet-50, AlexNet for KOA detection Key Findings KOA severity classification using CNN models and KL grading

Johanne Martel-Pelletier et.al (2022) [42]	MRI-based evaluation of knee tissues and machine learning for KOA prediction Methodology MRI-based knee tissue evaluation, deep learning Key Findings MRI-based approaches enhance early KOA diagnosis
Jianfeng Yang et.al (2022) [43]	RefineDet-based deep learning model for KOA diagnosis using X-ray images Methodology RefineDet deep learning model, KL grading Key Findings RefineDet model achieved high accuracy in KOA detection
Woon-Man Kung et.al (2021) [44]	Deep-KOA risk prediction model using ANN and CNN on NHIRD dataset Methodology ANN, CNN-based risk prediction using NHIRD data Key Findings Deep learning model achieved high AUROC in KOA prediction
Pauline Shan Qing Yeoh et.al (2021) [2]	3D CNN applications for volumetric knee joint assessment in KOA diagnosis Methodology 3D CNN for volumetric knee joint imaging Key Findings 3D CNN provides enhanced KOA diagnostic accuracy
Aleksei Tiulpin et.al (2018) [45]	Deep Siamese CNN for automated KL grading of KOA severity Methodology Siamese CNN for KL grading of KOA Key Findings 66.71% accuracy with Siamese CNN, Kappa coefficient of 0.83
Serafeim Moustakidis et.al (2018) [46]	Machine learning for non-invasive identification of KOA risk factors Methodology Machine learning for KOA risk factor identification Key Findings Deep learning identified KOA risk factors with 86.95% accuracy
Turgay Ibrikci et.al (2017) [3]	Surface electromyography-based detection of KOA using pattern recognition Methodology Electromyography, pattern recognition, deep learning Key Findings Non-invasive KOA detection with electromyography and AI

III. METHODOLOGY

Discrete-MultiResUNet Architecture for Bone Region Extraction

This work considers the Discrete-MultiResUNet model and its utilization in bone region initialization, boundary leakage correction, and feature extraction using Discrete Wavelet Transform (DWT). The model utilizes multi-resolution techniques to aid in enhancing the bone region segmentation process of medical images, in contrast to usual limitations of boundary leakage and requirement for robust feature extraction mechanisms.

Discrete-MultiResUNet Architecture

The Discrete-MultiResUNet is a visual segmentation deep C.N.N. This is a continuation of that basic U-Net architecture with the addition of multi-resolution pathways to capture more precise feature representation at multiple scales. In the field of medicine, this is especially helpful because the object causes concern, for instance, bones, can have significantly varying size and shape.

Key Features:

- Multi-Resolution Pathways: The architecture processes input images at multiple resolutions, enabling it to capture both fine and coarse details.

- Skip Connections: These connections between encoder and decoder layers help retain spatial information, which is crucial for accurate segmentation.
- Attention Mechanisms: Optional attention layers can be integrated to focus on relevant features, further improving segmentation performance.

Initialization of Bone Region Extraction

The initialization of bone region extraction involves pre-processing steps that prepare the input data for effective segmentation. This includes normalization, resizing, and possibly dataset augmentation to enhance the robustness of the model.

Steps for Initialization:

1. Data Pre-processing: Scale the intensity values of the images so that the model has consistent input.
2. Resizing: Resize the image sizes to conform to the input size accepted by the Discrete-MultiResUNet.
3. Data Augmentation: Use methods like Scale, turning & rotational to increase instructional variability data.

Boundary Leakage Correction

Boundary leakage is a common image segmentation phenomenon wherein the model is unable to correctly predict the edges of the areas of interest. In an effort to solve this, the Discrete-MultiResUNet applies various approaches:

Techniques for Boundary Leakage Correction:

- Post-Processing: Implement morphological operations to refine the predicted boundaries after the initial segmentation.
- Loss Function Adjustment: Utilize loss functions that emphasize boundary accuracy, such as Dice loss or boundary-aware loss functions.
- Training with Boundary Masks: Incorporate boundary masks during training to guide the model in learning more precise boundary delineations.

Feature Extraction using DWT

Discrete Wavelet Transform (DWT) is a versatile feature extraction technique, especially used in medical imaging. It decomposes images in various frequency components so that both high-frequency features and low-frequency trends can be captured by the model.

Steps for Feature Extraction:

1. Wavelet Decomposition: Perform DWT on the given images to acquire different frequency sub-bands.
2. Feature Selection: Choose and pick suitable characteristics of the coefficients of wavelets that are essential to the segmentation process.

Integrating with Discrete-MultiResUNet: Integrate the features with the Discrete-MultiResUNet structure to improve the latter's bone region extraction capability.

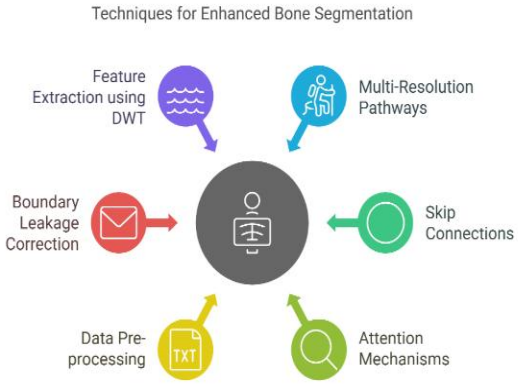

Figure 3: Techniques for enhanced bone segmentation

D. Discrete-Multi ResUNet Architecture (Source: Author)

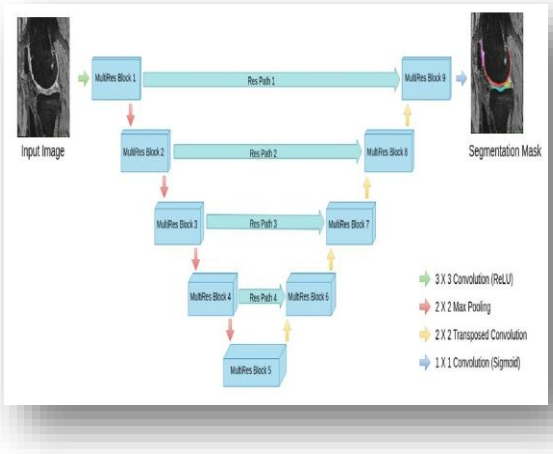

Figure 4: Proposed segmentation architecture

The proposed MultiResUNet structure enhances U-Net for the proper execution of segmentation tasks. The structure is modified according to the given

task, involving a 3 x 3 convolutional layer, a 2 X 2 max pooling process, a 2 X 2 transposed convolution, and a 1 X 1 sigmoid activation function. The model convolution is equipped with a rectifier linear unit to ensure the effectiveness of the segmentation job (ReLU). The wavelet transform is used to provide spatial support during the feature extraction process. To evaluate the image's characteristics, the segmented image is split into sub-bands. Despite previous methods, wavelet transformations allow for signal time-frequency localization.

E. Initialization of Bone Region Extraction

The first bone segments belonging to the femur and tibia are retrieved through using MultiResUNet architecture, which includes automated seed point determination. The seed points generated from the 3D overlapped technique are first utilized to build an appropriate level in MultiResUNet, which develops across the femur and tibia bone areas and retrieves initial bone sections from the MR image. After that, the bone areas are extended further to identify geometrical coordinates. The coordinates found is then utilized to initialize the subsequent slices. This method is repeated for the entire dataset, and geometrical coordinates are updated for every slice taken from the femur and tibia bone areas. If the thresholding goes below a specific level, the algorithm ends the bone region's initialization procedure. Figure 5 depicts roughly 40 bone-free slices at the commencement and conclusion of the slice series. When the region of the femur and tibia bone slices becomes less than 100 pixels, the procedure immediately ends.

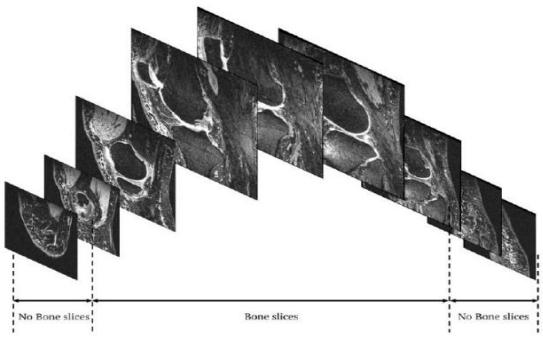

Figure 5: Slices consisting of bone and no-bone regions

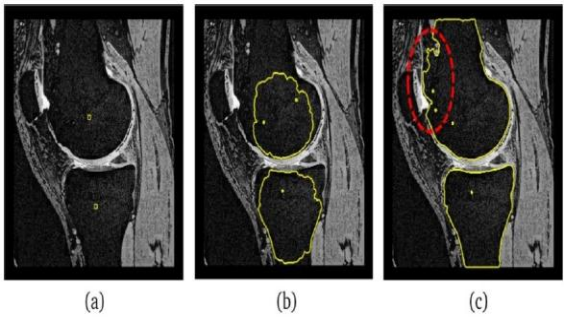

Figure 6: Bone region extraction (a) Seed selection, (b) Intermediate stage, (c) Final stage of bone region extraction

Figure 6 depicts the extraction of a bone area using an automated seed selection technique. Other tissues, in addition to bone areas, are retrieved in this illustration. These other tissues are corrected or removed during post processing process. Once the bone region is corrected then the remaining region is masked to obtain the joint space narrowing (JSN) between femur and tibia.

F. Boundary Leakage Correction

Point-to-point endpoints are calculated by calculating the distance between both the present and subsequent endpoints in two successive slices. The variation in bone tissue architecture is quite tiny and changes gradually. Distances that exceed a predetermined threshold are labeled as leakages, and they are rectified by moving the points corresponding to the outliers from the neighboring border. The proposed boundary correction is provided in following equations. The current boundary coordinates (Bcur), and adjacent boundary coordinates (Badj) are shown as follows in equation.

$$B_{cur} = \{x, y | (x_i, y_i), i = 1{:}N\}$$

$$B_{adj} = \{x, y | (x_i, y_i), j = 1{:}M\}$$

Where x, y are the bone's coefficient vectors and M, N are the number of Cartesian coordinates in the neighboring and contemporary boundaries, appropriately. To calculate the point-to-point proximity, the number of data points in each dataset is equalized utilizing normal approximation. As indicated in equation 4.3, the distance amongst consecutive slice boundaries is calculated using Euclidean distance.

$$E(dist) = dist\left(B_{cur}, B_{adj}\right)$$
$$= \sqrt{(Y_{cur} - Y_{adj})^2 + (X_{cur} - X_{adj})^2}$$

Algorithm 1. Boundary Correction and displacement
Input: MR slices Output: Boundary corrected and masked MR slice 1. Determine the set of boundary parameters for an MR slice. 2. Interpolate the points to make equal slices. 3. Using equation 4.3, calculate the point-to-point distance between the two coordinates. 4. Applying equations (4.4, 4.5, 4.6, 4.7), categorize points as outlier or non-outliers. 5. If the outlier points are set as null ($P(cur)_o = \emptyset$), then go to step 8, else go to step 5. 6. Using equations (4.10, 4.11), reposition the endpoints in the slice that corresponds to the outlier by$d(dis)$. 7. Applying equation 4.15, incorporate the relocated endpoints from the slice with the non-outlier set of endpoints. 8. Populate in any boundary gap that exists to obtain a final adjusted contour. 9. Repeating steps 1–7 to adjust the boundaries all throughout dataset.

G. Feature Extraction using DWT

The proposed architecture uses discrete wavelet transforms (DWT) for extracting the features from segmented image. Higher - level wavelet coefficients are adjusted, and the continuous wavelet transformation f(x) and real – valued discrete wavelet function f(x) are used Ψ(x), is described in equation 4.1. In equation the scaled and transition parameters are represented as s and t respectively. The wavelet function Ψs,t(x) is generated from Ψ(.), by constraining s and t to a discrete lattice with s=2j and t=2jk.

$$W_\Psi(s,t) = \int_{-\infty}^{\infty} f(x)\Psi_{s,t}(x)dx$$

Where,

$$\Psi_{s,t}(x) = \frac{1}{\sqrt{s}}\Psi\left(\frac{x-t}{s}\right); s\epsilon\Re, t\epsilon\Re$$

$$DWT_{f(n)} = \begin{cases} A_{j,k}(n) = \sum_n f(n)G_j^*(n-2^jk) \\ D_{j,k}(n) = \sum_n f(n)H_j^*(n-2^jk) \end{cases}$$

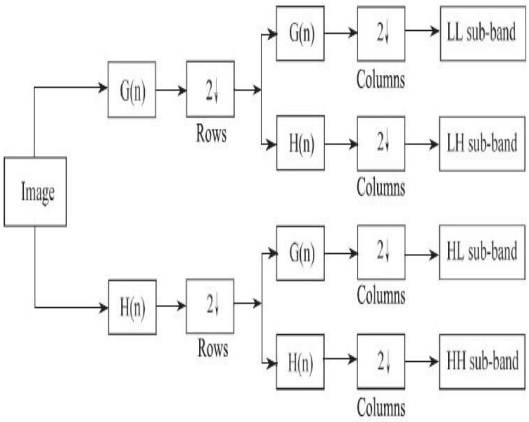

Figure 7: 2D discrete wavelet transform

Figure 7 depicts the images adhered to every dimension individually into rows and columns of the image after it has been subjected to linear and two-dimensional Wavelet transform. As a consequence, four bands are produced to get pictures at every level (LL: low-low, LH: low-high, HL: high-low, HH: high-high).Images from three specific sub-bands are included, LH (D_j^h), HL (D_j^v), HH (D_j^d) are detailed images that run horizontally, vertically, and diagonally. The approximation image applied for two-dimensional estimation at the following level is LL (A_j) sub-band. Figure 8 depicts a knee MR image with a two-channel discrete wavelet transform.

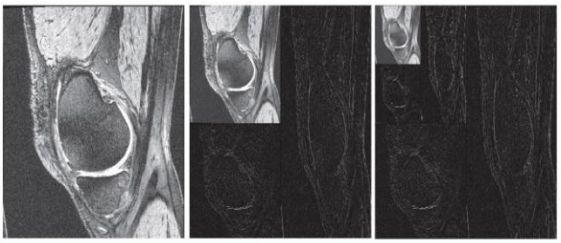

Figure 8: Knee MR Image with wavelet transforms coefficient at two-channel decomposition.

There are several varieties of wavelet transforms, the most common of which being the Harr wavelet. Because the Harr wavelet is both orthogonal and symmetrical, it produces satisfactory accuracy. Furthermore, it is computationally efficient when extracting morphological information from the images. In this dissertation, we analyzed and calculated the two-channel decomposition of the Harr wavelet as a feature vector (FV) for every image. By aggregating all of the FV from N pictures, an approximate feature vector of size N X M Comprising M features with each image is

generated. Algorithm 2 shows the processes for creating a feature extraction matrix.

The feature vector obtained by the two-channel decomposition is pretty excellent and result in higher computational efficiency. To address the issue of the system's reduced capability to deal with missing information, feature normalization is employed, thereby boosting the overall efficiency of the system. For example, if the image size is 256 X 256, the feature vector size is 32 X 32 = 1024. In general, all characteristics are irrelevant for categorization and are utilized to reduce the dimensionality. Algorithm 3 depicts the feature normalization algorithm. The techniques of two-channel dimensionality of the Harr wavelet for feature extraction decrease the number of parameters to 32 X 32 = 1024. These major characteristics are merely normalized while maintaining the same quantity of features, i.e., 1024. However, the feature vector size is still too huge and therefore should be minimized.

As a consequence, feature reduction is often used to reduce the dimension of the feature vector. Algorithm 4 depicts the feature reduction.

IV. RESULTS AND DISCUSSION

To illustrate the experimental observations, the proposed ResNet50 technique's performance was evaluated with a variety of characteristics such as confusion matrix, efficiency, precision, sensitivity, specificity, F1-measure, mean absolute error (MAE), and joint space narrowing (JSN). Purpose of providing linearity in training using Adam optimizer, the dataset is generally split by k-fold cross validation. The training rate was set to 0.001, while the weight decaying was adjusted to 0.0001. The proposed research performed on an Intel core i3-7130U Processor operating at 2.70GHz with 12 GB RAM. The dataset was classified by the model based on its KL classification / scoring. If the JSN value is zero, the arthritis is labelled as grade 0; if the JSN value is less than 10%, the arthritis is labelled as grade 1, (doubtful arthritis). If the JSN value is between 11% and 25%, it is labelled as mild arthritis; if it is between 26% and 75%, it is labelled as moderate arthritis; and if it is higher than 75%, it is labelled as degenerative arthritis (severe arthritis).

Table 2 demonstrates the datasets used for analysis of results for progression of arthritis. First dataset was collected from local hospital and second collected from Osteoarthritis Initiative (OAI) database. The local dataset was a raw data so, needed to be pre-process as discussed in chapter 3. The OAI dataset was a pre-processed data so directly used for experiments. Both datasets were consisting of different training, testing and validation samples. The data was divided according to k-fold cross validation approach into training set (70%), validation (10%), and testing set (20%).

Table 2: Datasets used for experimental analysis.

Dataset	Local			OAI		
	Training	Testing	Validation	Training	Testing	Validation
Grade 0	10115	2578	1193	2286	639	328
Grade 1	7132	1783	967	1046	296	153
Grade 2	5256	1329	650	1516	447	212
Grade 3	4379	1052	508	757	223	106
Grade 4	4833	1186	624	173	51	27

As the proposed architecture uses transfer learning that helps in convergence of deep learning model (ResNet50). Table 3 describes the performance parameters used for local dataset. The JSN values for grades from 0 to 4 are well estimated and grade 4 has value of 0.99. The proposed model achieved sensitivity of 0.97 on an average value for all grades. The specificity achieved for grade 1 and grade 4 are 0.84 and 0.92 respectively. The model also achieved an accuracy of 97.98%, 95.50%, 95.26%, 96.73%, and 98.15%, for grade 0, 1, 2, 3, and 4 respectively. The MAE estimated was 0.092 and 0.203 for grade 0 and grade 2 respectively. Table 4 describes the performance parameters used for OAI dataset.

Table 3: Different performance parameters with KL grade on local dataset.

KL grades	JSN	Precision (%)	Sensitivity	Specificity	F1-score	Accuracy (%)	MAE	AUC
Grade 0	0.98	0.99	0.97	0.90	0.98	97.98	0.092	0.97
Grade 1	0.98	0.95	0.98	0.84	0.97	95.50	0.197	0.96
Grade 2	0.97	0.95	0.98	0.87	0.97	95.26	0.203	0.96
Grade 3	0.98	0.98	0.97	0.86	0.98	96.73	0.119	0.97
Grade 4	0.99	0.99	0.99	0.92	0.99	98.15	0.088	0.97

Table 4: Different performance parameters with KL grade on OAI dataset.

KL grades	JSN	Precision (%)	Sensitivity	Specificity	F1-score	Accuracy (%)	MAE	AUC

Grade 0	0.96	0.97	0.96	0.91	0.96	97.68	0.082	0.97
Grade 1	0.96	0.97	0.97	0.86	0.97	96.37	0.317	0.97
Grade 2	0.95	0.95	0.96	0.85	0.98	96.76	0.283	0.96
Grade 3	0.96	0.98	0.97	0.87	0.97	97.10	0.039	0.97
Grade 4	0.98	0.98	0.98	0.88	0.98	98.77	0.028	0.97

Table 5 provides a comparative analysis of several techniques used to address femoral and tibial tissues, wherein L indicates lateral, and M represents medial. Only the medial and lateral compartments of femoral and tibial tissue are examined. The proposed architecture achieved an accuracy of 96.85% which is quite good compared to other existing techniques. The residual network of 34 layers (ResNet34) also achieved goo results with an accuracy of 94.39% which is near to proposed architecture negative sample images were 3245. Table 6 shows some parameters such as false negative and positive rate that are 0.0378 and 0.0229 respectively. It also has a coefficient of correlation of 0.9258 and a false discovery rate of 0.0169.

Table 5: Comparative analysis of different techniques related to lateral and medial femur and tibia tissue with JSN value.

Techniques	Femur		Tibia		JSN		Accuracy (%)	MAE
	L	M	L	M	L	M		
SVM	0.71	0.73	0.78	0.77	0.91	0.87	86.53	0.319
RF	0.68	0.69	0.80	0.78	0.90	0.87	87.84	0.308
VGG	0.84	0.81	0.82	0.79	0.91	0.87	90.45	0.216
CNN	0.83	0.84	0.82	0.79	0.91	0.87	91.89	0.285
Dense-Net	0.85	0.84	0.83	0.80	0.92	0.88	93.77	0.270
ResNet34	0.86	0.86	0.84	0.82	0.92	0.88	94.39	0.216
Proposed Model	0.88	0.86	0.86	0.89	0.93	0.91	96.85	0.105

The Dense-Net model gained good result for lateral JSN value of 0.92.For the lateral compartment, the support vector machine (SVM), oxford Net (VGG), and convolutional neural network (CNN) methods simultaneously obtained a really reasonable result of 0.91. The random forest (RF) gained less attention for every compartment analysed. Table 6 illustrates the performance measures achieved for proposed model. Figure 9 illustrates the confusion matrix estimated for proposed model. The confusion matrix illustrates the classification model's performance on the testing dataset. The true-positive were 4433 knee MR images.

Table 6: Performance parameters achieved for proposed model.

Performance parameters	Obtained value
Sensitivity or Recall	0.9622
Specificity	0.9771
Precision	0.9831
Negative predicted value	0.9491
False-positive rate	0.0229
False discovery rate	0.0169
False-negative rate	0.0378
Accuracy	0.9685
F1 score	0.9726
Matthew's correlation coefficient	0.9258

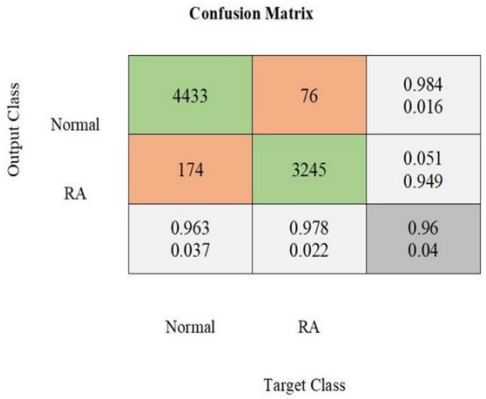

Figure 9: Confusion matrix for proposed architecture (ResNet50)

V. CONCLUSION

The proposed study faces several limitations that warrant consideration. Firstly, the validation dataset was included in the training process, which may introduce bias and affect the generalizability of the model. Excluding this data could have provided a more robust evaluation of the model's performance. Despite this limitation, the developed model demonstrated superior clinical performance, exhibiting higher classification efficiency for early osteoarthritis (OA) assessment compared to other models.

The other limitation is decreased image quality, which can lead to loss of fine-grained detail in the images. Resolution increase and the addition of more information could possibly improve the output of the model. In addition, discrepancies between model classification and expert KL grading estimates suggest potential inaccuracies in the labelling of the dataset. This underlines the need for

thorough validation and calibration of the KL grading system in OA datasets.

Additionally, model performance may also be further improved by taking up a novel loss function best able to utilize an abundance of information from diverse sources during learning. This will increase the model's accuracy and reliability in estimating OA severity. Other than that, photos employed within the study were taken under controlled conditions with the assistance of a positioning frame, thereby restricting unadulterated application of the technique to other healthcare environments. Additional efforts are required in order to scale down and fine-tune the technique for further use outside of the OAI and local databases.

In spite of these constraints, the suggested approach has some advantages for the medical community. By facilitating the provision of individual KL grade likelihood estimates, the model can help clinicians properly diagnose and treat OA cases with the aim of minimizing costs and enhancing the patient outcome. The scientific community can also employ the suggested model as an economical means to process large databases and interpret the medical images associated with OA.

VI. REFRENCES

[1] D. Saini, T. Chand, D. K. Chouhan, and M. Prakash, "A comparative analysis of automatic classification and grading methods for knee osteoarthritis focussing on X-ray images," Biocybernetics and Biomedical Engineering, vol. 41, no. 2, pp. 419–444, Apr. 2021, doi: 10.1016/j.bbe.2021.03.002.

[2] [P. S. Q. Yeoh et al., "Emergence of Deep Learning in Knee Osteoarthritis Diagnosis," Computational Intelligence and Neuroscience, vol. 2021, no. 1, p. 4931437, Jan. 2021, doi: 10.1155/2021/4931437.

[3] J. de D. Uwisengeyimana and T. Ibrikci, "Diagnosing Knee Osteoarthritis Using Artificial Neural Networks and Deep Learning," 2017, doi: doi: 10.11648/j.bsi.20170203.11.

[4] J. Martel-Pelletier, P. Paiement, and J.-P. Pelletier, "Magnetic resonance imaging assessments for knee segmentation and their use in combination with machine/deep learning as predictors of early osteoarthritis diagnosis and prognosis," Therapeutic Advances in Musculoskeletal, vol. 15, p. 1759720X231165560, Jan. 2023, doi: 10.1177/1759720X231165560.

[5] Y. X. Teoh et al., "Discovering Knee Osteoarthritis Imaging Features for Diagnosis and Prognosis: Review of Manual Imaging Grading and Machine Learning Approaches," Journal of Healthcare Engineering, vol. 2022, pp. 1–19, Feb. 2022, doi: 10.1155/2022/4138666.

[6] F. Calivà, N. K. Namiri, M. Dubreuil, V. Pedoia, E. Ozhinsky, and S. Majumdar, "Studying osteoarthritis with artificial intelligence applied to magnetic resonance imaging," Nat Rev Rheumatol, vol. 18, no. 2, pp. 112–121, Feb. 2022, doi: 10.1038/s41584-021-00719-7.

[7] N. Sharma, R. Sapra, Sarita, and P. Dhaliwal, "A Comprehensive Review on Knee Osteoarthritis Detection using Medical Imaging and Machine Learning," in 2024 International Conference on Intelligent Systems for Cybersecurity (ISCS), Gurugram, India: IEEE, May 2024, pp. 1–6. doi: 10.1109/ISCS61804.2024.10581051.

[8] R. Fitriati, "Osteoarthritis," KESANS, vol. 1, no. 4, pp. 415–421, Jan. 2022, doi: 10.54543/kesans.v1i4.42.

[9] A. Mobasheri et al., "Osteoarthritis Research Society International (OARSI): Past, present and future," Osteoarthritis and Cartilage Open, vol. 3, no. 2, p. 100146, Jun. 2021, doi: 10.1016/j.ocarto.2021.100146.

[10] A. Xuan et al., "The application of machine learning in early diagnosis of osteoarthritis: a narrative review," Therapeutic Advances in Musculoskeletal, vol. 15, p. 1759720X231158198, Jan. 2023, doi: 10.1177/1759720X231158198.

[11] Z. Zhao et al., "Identifying significant structural factors associated with knee pain severity in patients with osteoarthritis using machine learning," Sci Rep, vol. 14, no. 1, p. 14705, Jun. 2024, doi: 10.1038/s41598-024-65613-0.

[12] A. Tiulpin, "Deep learning for knee osteoarthritis diagnosis and progression prediction from plain radiographs and clinical data," 2020, [Online]. Available: https://urn.fi/URN:ISBN:9789526225524

[13] Y. Xin Teoh, A. Othmani, S. Li Goh, J. Usman, and K. W. Lai, "Deciphering Knee

Osteoarthritis Diagnostic Features With Explainable Artificial Intelligence: A Systematic Review," IEEE Access, vol. 12, pp. 109080–109108, 2024, doi: 10.1109/ACCESS.2024.3439096.

[14] J. A. Roman-Blas and S. A. Jimenez, "NF-κB as a potential therapeutic target in osteoarthritis and rheumatoid arthritis," Osteoarthritis and Cartilage, vol. 14, no. 9, pp. 839–848, Sep. 2006, doi: 10.1016/j.joca.2006.04.008.

[15] B. Ravi et al., "A systematic review and meta-analysis comparing complications following total joint arthroplasty for rheumatoid arthritis versus for osteoarthritis," Arthritis & Rheumatism, vol. 64, no. 12, pp. 3839–3849, Dec. 2012, doi: 10.1002/art.37690.

[16] A. Jamshidi, J.-P. Pelletier, and J. Martel-Pelletier, "Machine-learning-based patient-specific prediction models for knee osteoarthritis," Nat Rev Rheumatol, vol. 15, no. 1, pp. 49–60, Jan. 2019, doi: 10.1038/s41584-018-0130-5.

[17] Y. Shi et al., "Advancing precision rheumatology: applications of machine learning for rheumatoid arthritis management," Front. Immunol., vol. 15, p. 1409555, Jun. 2024, doi: 10.3389/fimmu.2024.1409555.

[18] H. Zmerly et al., "Personalized Physical Activity Programs for the Management of Knee Osteoarthritis in Individuals with Obesity: A Patient-Centered Approach," Diseases, vol. 11, no. 4, p. 182, Dec. 2023, doi: 10.3390/diseases11040182.

[19] H.-S. Gan, M. H. Ramlee, A. A. Wahab, Y.-S. Lee, and A. Shimizu, "From classical to deep learning: review on cartilage and bone segmentation techniques in knee osteoarthritis research," Artif Intell Rev, vol. 54, no. 4, pp. 2445–2494, Apr. 2021, doi: 10.1007/s10462-020-09924-4.

[20] K. D. Allen, L. M. Thoma, and Y. M. Golightly, "Epidemiology of osteoarthritis," Osteoarthritis and Cartilage, vol. 30, no. 2, pp. 184–195, Feb. 2022, doi: 10.1016/j.joca.2021.04.020.

[21] K. S. Hemanth, D. Tigulla, V. Lakshmi, and S. Buhari, "Early stage detection of osteoarthritis of the joints (hip and knee) using machine learning," in Diagnosing Musculoskeletal Conditions using Artifical Intelligence and Machine Learning to Aid Interpretation of Clinical Imaging, Elsevier, 2025, pp. 39–64. doi: 10.1016/B978-0-443-32892-3.00003-8.

[22] K. Leung et al., "Prediction of Total Knee Replacement and Diagnosis of Osteoarthritis by Using Deep Learning on Knee Radiographs: Data from the Osteoarthritis Initiative," Radiology, vol. 296, no. 3, pp. 584–593, Sep. 2020, doi: 10.1148/radiol.2020192091.

[23] C. Prabha, "Early detection approach for analysis of osteoarthritis using artificial intelligence and machine learning," in Diagnosing Musculoskeletal Conditions using Artifical Intelligence and Machine Learning to Aid Interpretation of Clinical Imaging, Elsevier, 2025, pp. 147–165. doi: 10.1016/B978-0-443-32892-3.00008-7.

[24] S. M. Ahmed and R. J. Mstafa, "Identifying Severity Grading of Knee Osteoarthritis from X-ray Images Using an Efficient Mixture of Deep Learning and Machine Learning Models," Diagnostics, vol. 12, no. 12, p. 2939, Nov. 2022, doi: 10.3390/diagnostics12122939.

[25] S. M. Ahmed and R. J. Mstafa, "A Comprehensive Survey on Bone Segmentation Techniques in Knee Osteoarthritis Research: From Conventional Methods to Deep Learning," Diagnostics, vol. 12, no. 3, p. 611, Mar. 2022, doi: 10.3390/diagnostics12030611.

[26] G. Açar and A. E. Çiçek, "Review of Clinical Anatomy Researches," Mar. 26, 2024, Livre de Lyon. doi: 10.5281/ZENODO.10875967.

[27] S. Jang, K. Lee, and J. H. Ju, "Recent Updates of Diagnosis, Pathophysiology, and Treatment on Osteoarthritis of the Knee," IJMS, vol. 22, no. 5, p. 2619, Mar. 2021, doi: 10.3390/ijms22052619.

[28] J. C. Mora, R. Przkora, and Y. Cruz-Almeida, "Knee osteoarthritis: pathophysiology and current treatment modalities," JPR, vol. Volume 11, pp. 2189–2196, Oct. 2018, doi: 10.2147/JPR.S154002.

[29] R. Marks, "Knee Joint Neural Sources and Pathways and Their Osteoarthritis Pathogenic Linkages and Pain Control Implications," JOSR, pp. 1–11, Jul. 2024, doi: 10.46889/JOSR.2024.5205.

[30] Krishna Pramanik, Stem Cell and Tissue Engineering: Bone, Cartilage, and Associated Joint Tissue Defects. 2024.

[31] Rishabha Malviya, Artificial Intelligence for Bone Disorder Diagnosis and Treatment. 2024.

[32] Y. Jiang and R. S. Tuan, "Origin and function of cartilage stem/progenitor cells in osteoarthritis," Nat Rev Rheumatol, vol. 11, no. 4, pp. 206–212, Apr. 2015, doi: 10.1038/nrrheum.2014.200.

[33] Musumeci, "Age-related degeneration of articular cartilage in the pathogenesis of osteoarthritis: molecular markers of senescent chondrocytes," Histology and Histopathology, no. 30, pp. 1–12, Dec. 2014, doi: 10.14670/HH-30.1.

[34] S. Rani et al., "Deep learning to combat knee osteoarthritis and severity assessment by using CNN-based classification," BMC Musculoskelet Disord, vol. 25, no. 1, p. 817, Oct. 2024, doi: 10.1186/s12891-024-07942-9.

[35] P. M. Dinesh, K. Kumar Govindaraj, N. Manivannan, M. E. Paramasivam, P. William, and M. Alagarsamy, "Deep Learning-Based Prediction of Knee Innovative Practices," in 2024 4th International Conference on Innovative Practices in Technology and Management (ICIPTM), Noida, India: IEEE, Feb. 2024, pp. 1–6. doi: 10.1109/ICIPTM59628.2024.10563465.

[36] A. Rafiq et al., "Detection and Classification of Histopathological Breast Images Using a Fusion of CNN Frameworks," Diagnostics, vol. 13, no. 10, p. 1700, May 2024, doi: 10.3390/diagnostics13101700.

[37] J. S. Yoon et al., "Assessment of a novel deep learning-based software developed for automatic feature extraction and grading of radiographic knee osteoarthritis," BMC Musculoskelet Disord, vol. 24, no. 1, p. 869, Nov. 2023, doi: 10.1186/s12891-023-06951-4.

[38] N. Rameez, G. G. D. Dissanayake, G. A. C. Senindu, P. M. H. Liyanage, and V. Embuldeniya, "Knee Osteoarthritis Detection Using Machine Learning on Pre-Processed X-ray Images and Treatment Recommendation," in 2024 8th SLAAI International Conference on Artificial Intelligence (SLAAI-ICAI), Ratmalana, Sri Lanka: IEEE, Dec. 2024, pp. 1–6. doi: 10.1109/SLAAI-ICAI63667.2024.10844957.

[39] A. Haseeb et al., "Knee Osteoarthritis Classification Using X-Ray Images Based on Optimal Deep Neural Network," Computer Systems Science and Engineering, vol. 47, no. 2, pp. 2397–2415, 2023, doi: 10.32604/csse.2023.040529.

[40] J. Song and R. Zhang, "A novel computer-assisted diagnosis method of knee osteoarthritis based on multivariate information and deep learning model," Digital Signal Processing, vol. 133, p. 103863, Mar. 2023, doi: 10.1016/j.dsp.2022.103863.

[41] R. N. Kadu, S. N. Pawar, and S. A. Shaikh, "A Comprehensive Review on Advances in Detection of Knee Osteoarthritis," in Multi-Strategy Learning Environment, V. Vimal, I. Perikos, A. Mukherjee, and V. Piuri, Eds., in Algorithms for Intelligent Systems. , Singapore: Springer Nature Singapore, 2024, pp. 315–327. doi: 10.1007/978-981-97-1488-9_24.

[42] G. Tardif et al., "Mass spectrometry-based proteomics identify novel serum osteoarthritis biomarkers," Arthritis Res Ther, vol. 24, no. 1, p. 120, Dec. 2022, doi: 10.1186/s13075-022-02801-1.

[43] J. Yang, Q. Ji, M. Ni, G. Zhang, and Y. Wang, "Automatic assessment of knee osteoarthritis severity in portable devices based on deep learning," J Orthop Surg Res, vol. 17, no. 1, p. 540, Dec. 2022, doi: 10.1186/s13018-022-03429-2.

[44] D. N. A. Ningrum et al., "A Deep Learning Model to Predict Knee Osteoarthritis Based on Nonimage Longitudinal Medical Record," JMDH, vol. Volume 14, pp. 2477–2485, Sep. 2021, doi: 10.2147/JMDH.S325179.

[45] A. Tiulpin, J. Thevenot, E. Rahtu, P. Lehenkari, and S. Saarakkala, "Automatic Knee Osteoarthritis Diagnosis from Plain Radiographs: A Deep Learning-Based Approach," Sci Rep, vol. 8, no. 1, p. 1727, Jan. 2018, doi: 10.1038/s41598-018-20132-7.

[46] S. Moustakidis, E. Christodoulou, E. Papageorgiou, C. Kokkotis, N. Papandrianos, and D. Tsaopoulos, "Application of machine intelligence for osteoarthritis classification: a classical implementation and a quantum perspective," Quantum Mach. Intell., vol. 1, no. 3–4, pp. 73–86, Dec. 2019, doi: 10.1007/s42484-019-00008-3.